wiscobolt
(validation)

Note: This document is a work-in-progress

Muhsin H. Younis

First published 10-21-23
Latest version: 0.1, published 10-21-23

Table of Contents

1 Validation of numerical methods: The method of manufactured solutions

In order to validate that we can solve the 5D monoenergetic Boltzmann transport equation, we use the method of manufactured solutions (MMS) [1, 2]. In the MMS, we decide on a solution ψ first, then determine the source s that corresponds to it by evaluating $\hat{L}\psi = s$, by hand where possible. Then, we discretize this source and feed that into our solver, and evaluate the solution against the discretized form of the known solution. We will use this method to validate the task of solving $T\psi = s$ alone as well as $L\psi = s$, where L is a monoenergetic BTE matrix. We evaluate cases which put stress on our discretization methods, as well as one which includes boundary conditions in the sweep.

1.1 Transport operator

1.1.1 Test case 1 (cube, steep gradient, vacuum boundary conditions)

In this problem, we look at a solution to the Boltzmann transport equation which has a relatively steep and tunable gradient. Our test problem is described by the 5D function:

$$\psi(\mathbf{r}, \hat{\mathbf{k}}) = e^{-\cos\phi} e^{\mu} e^{-A(x-1/2)^2} e^{-A(y-1/2)^2} \left[2 - \cosh(\alpha z - \alpha/2)\right] \tag{1.1.1}$$

where:

$$A = 100 \tag{1.1.2}$$

$$\alpha = 2\ln(2 + \sqrt{3}) \tag{1.1.3}$$

Qualitatively, A is a parameter which tunes the sharpness of the gradient. Notably, Σ_t is not present in ψ. Its value in this test case has been found to be generally not significant, as long as it is positive (a specification we are happy to make in Boltzmann transport). That said, when Σ_t is large relative to the matrix elements of the streaming operator $\hat{\mathbf{k}} \cdot \nabla$, we get $\psi \approx s/\Sigma_t$, and so our solver is meaninglessly accurate. We'll simply take $\Sigma_t = 1$. Additionally, it is noteworthy that every variable is completely separable. Finally, this solution with a large A approximately satisfies the boundary condition that $\bar{\psi} = 0$ (vacuum boundary conditions). It satisfies vacuum boundary conditions for $z = 0, 1$, but for $x = 0, 1$ or $y = 0, 1$ it will be on the order of $1.39 \cdot 10^{-11}$, which is acceptably small. The fluence associated with this function is:

$$\varphi(\mathbf{r}) = 7.9549(e^1 - e^{-1}) e^{-A(x-1/2)^2} e^{-A(y-1/2)^2} \left[2 - \cosh(\alpha z - \alpha/2)\right] \tag{1.1.4}$$

where the factor of 7.9549 results from integration of $e^{-\cos\phi}$ (it doesn't have a closed form). The normalized polar angle distribution of this function is:

$$f(\mu) = \frac{1}{e^1 - e^{-1}} e^{\mu} \tag{1.1.5}$$

Table 1: Discretization parameters for the first MMS problem. N_K is the total number of nodes in the mesh

Parameter	Mesh 1	Mesh 2	Mesh 3
N_E	46,821	90,643	229,943
N_K	9,248	16,218	38,634
N_μ	16	16	16
N_ϕ	32	32	32

Table 2: L2-norms of residuals for the first MMS problem.

	Mesh 1	Mesh 2	Mesh 3
$\lvert s - TT^{-1}s\rvert$	$1.36{\cdot}10^{-10}$	$2.42{\cdot}10^{-10}$	$1.07{\cdot}10^{-9}$

Now, the source for this problem is:

$$s(\mathbf{r}, \hat{\mathbf{k}}) = \psi(\mathbf{r}, \hat{\mathbf{k}}) \times \Bigg[\begin{array}{c} -A\sqrt{1-\mu^2}\cos\phi(2x-1) \\ -A\sqrt{1-\mu^2}\sin\phi(2y-1) \\ -\mu\alpha\frac{\sinh(\alpha z-\alpha/2)}{2-\cosh(\alpha z-\alpha/2)} \\ +\Sigma_t \end{array} \Bigg] \tag{1.1.6}$$

Note that, despite ψ being separable in every variable, s is not.

Discretization parameters for three different solves are shown in Table 1. The angular discretization parameters N_μ and N_ϕ refer to Gauss-Legendre and Gauss-Chebyshev sets respectively. Refer to Figure 1 for a selection of solved fluences and Figure 2 for the sources that result from wiscobolt applying the transport operator to an exact angular fluence, for a select discrete ordinate. That is, in the former, we display the fluence of $T^{-1}s$, and in the latter, $T\psi$ at a select discrete ordinate, where s and ψ are the exact quantities and T is the operator applied by wiscobolt. Then, in Figure 3, we show the difference of the calculated angular distributions from the exact angular distribution. Finally, in Table 2, we show the L2-norms of the residual, $\lvert s - TT^{-1}s\rvert_2$, which quantify that the sweep is in fact the inverse of T (as far as implementation, this is not necessarily intuitive, as application of T to some vector does not need to be done element-by-element in any particular order whereas T^{-1} does, so we are essentially verifying that our 'sweep' order is the correct one).

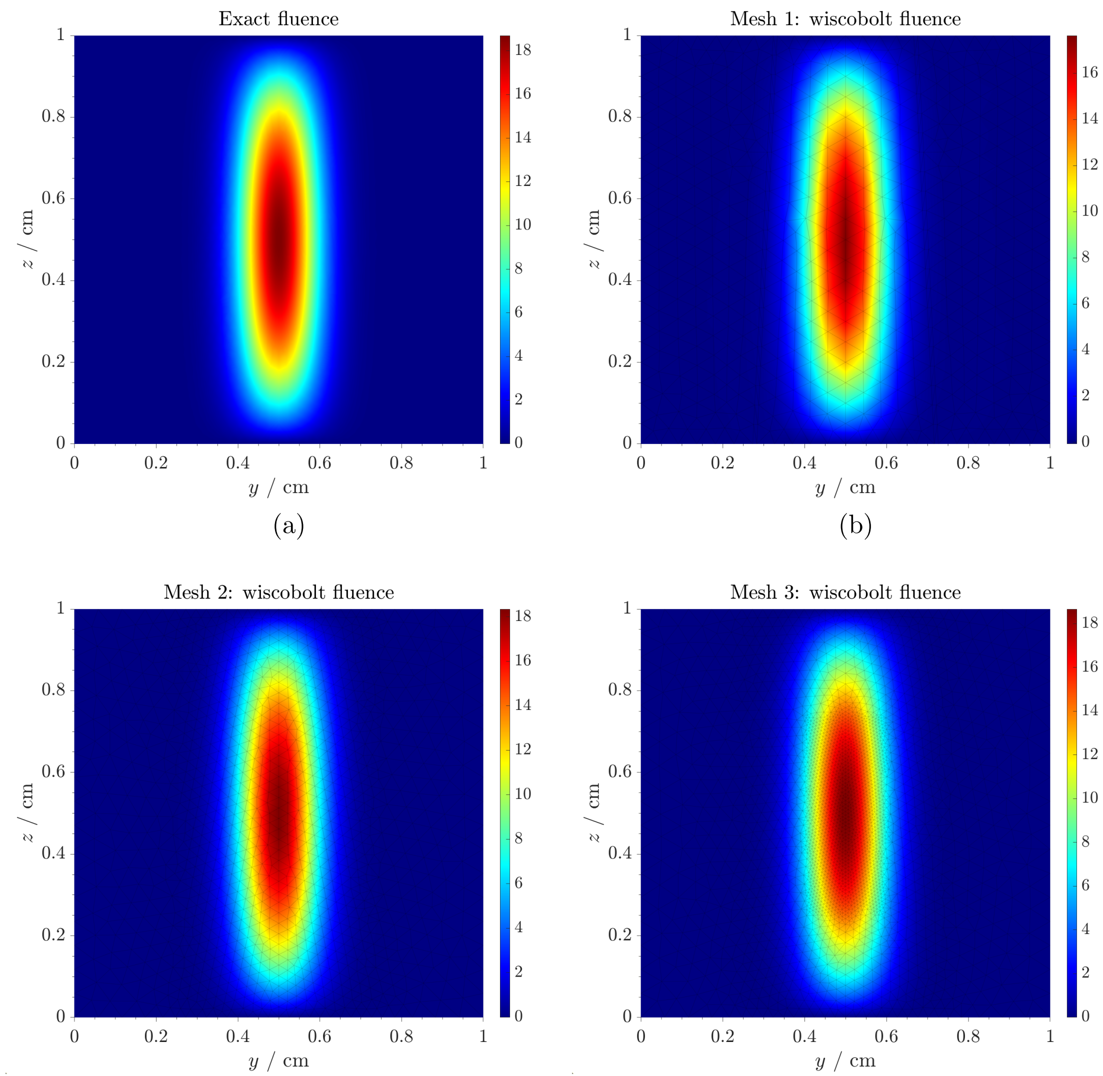

(a) (b) (c) (d)

Figure 1: Figures $(a)-(d)$ are, respectively, the exact fluence and the fluence solved by wiscobolt in meshes 1 thru 3. All mesh slices are in the $yz-$plane. 'Exact' quantities are plotted in the most refined mesh being used. Quantities resulting from wiscobolt are plotted with a translucent mesh grid, giving insight into the structure of the meshes, which are not generally uniform.

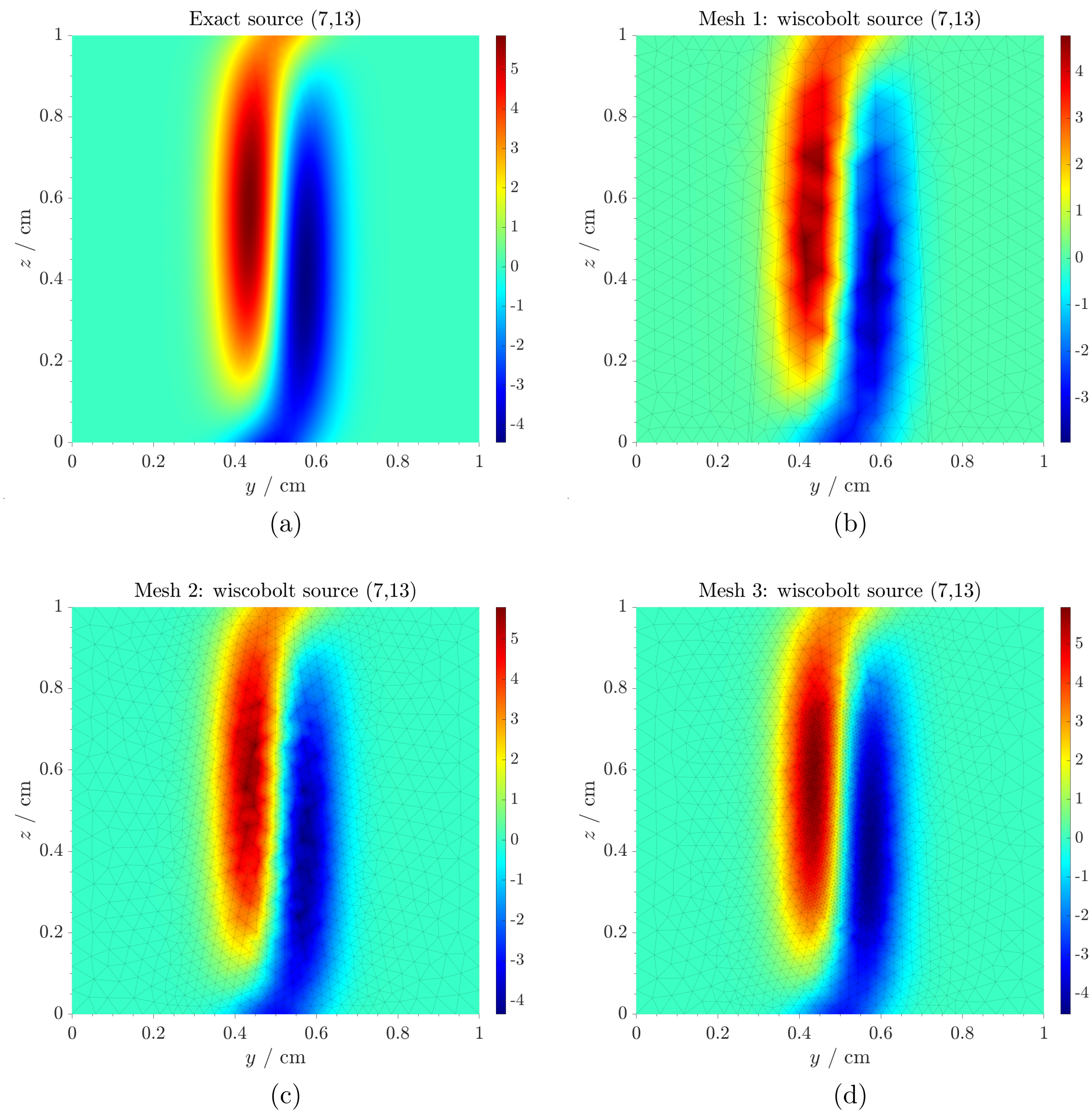

Figure 2: Figures $(a)-(d)$ are, respectively, the exact source and the source obtained by wiscobolt applying the transport operator to exact fluences in meshes 1 thru 3, at discrete ordinate $\hat{\mathbf{k}}_{7,13}$. The ordinate $(i, j) = (7, 13)$ is chosen in this problem because it represents a source term which is different in form from the solution, i.e., one that contains significant mixing of the derivatives of ψ.

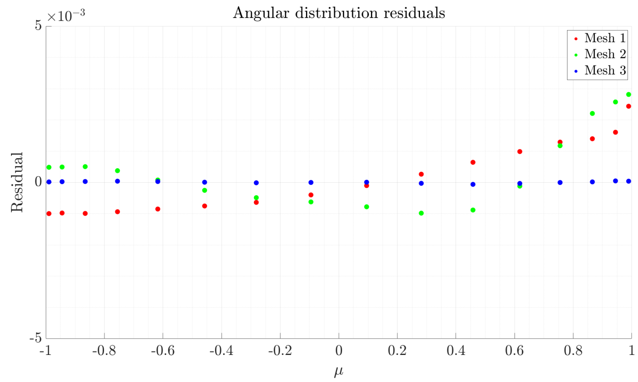

Figure 3: The residual of the angular distributions for the given meshes, i.e., the difference of the angular distribution from the exact angular distribution.

1.1.2 Test case 2 (sphere, small boundary conditions on incident faces)

In this test case, we are interested in demonstrating that boundary conditions can treat a case wherein the fluence on the incident boundary is small, whereas the outgoing boundary is much more appreciable. Notably, with non-reentrant boundary conditions, one does not specify any information for the outgoing boundary, only the incident boundary. That is, the boundary condition we are using is:

$$\psi(\mathbf{r},\hat{\mathbf{k}}) = \bar{\psi}(\mathbf{r},\hat{\mathbf{k}}),\ \hat{\mathbf{n}}(\mathbf{r})\cdot\hat{\mathbf{k}} < 0 \tag{1.1.7}$$

This says that we know ψ for points on the surface of our volume V, and angular coordinates $\hat{\mathbf{k}}$ such that at a given point in ∂V, $\hat{\mathbf{k}}$ is pointing into V. So, we know the solution for particles *entering* the volume. Now, our previous test cases satisfied $\bar{\psi} = 0$. But, they also satisfied $\psi = 0$ for *all* directions on the surface, not just directions entering the volume. So, we now ask: can our solver handle a solution which has nonzero fluence on the boundary for directions exiting the volume? We will perform this calculation on a sphere. The rationale for the construction of the following function is: we will take a 3D Gaussian centered at the origin of a sphere of radius R. This is just $e^{-|\mathbf{r}|^2}$. We will then translate it, for the direction $\hat{\mathbf{k}}$, a distance R along $\hat{\mathbf{k}}$. This amounts to $\mathbf{r} \to \mathbf{r} - R\hat{\mathbf{k}}$. Depending on how broad the Gaussian is, this should ensure that the boundary through which $\hat{\mathbf{k}}$ exits has nonzero fluence, while the boundary through which it enters has close to zero fluence. We will finally scale the argument of the exponent such that the value of ψ at $\mathbf{r} = -R\hat{\mathbf{k}}$ is given as some constant ε. Thus, we solve for the exponent's scaling constant C through:

$$e^{-4CR^2} = \varepsilon \tag{1.1.8}$$

Therefore, ε is a parameter that can tune the value of ψ at the incident boundary. We will use $\varepsilon = 10^{-3}$. We then find:

$$C = -\frac{1}{4R^2}\ln\varepsilon \tag{1.1.9}$$

Now, we have:

$$\psi(\mathbf{r},\hat{\mathbf{k}}) = e^{-C(\mathbf{r}-R\hat{\mathbf{k}})^2} \tag{1.1.10}$$

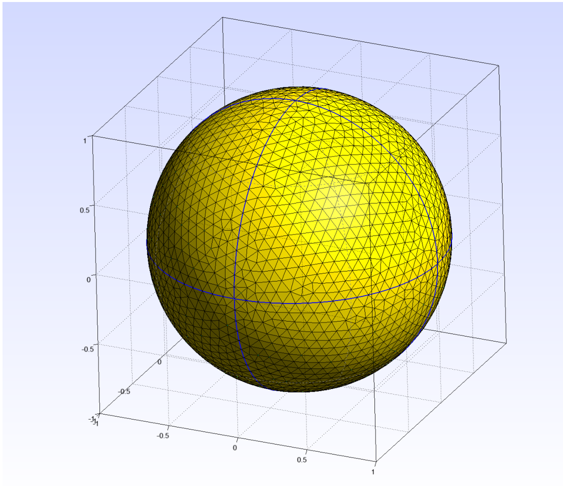

Figure 4: Mesh of a sphere, created with the Gmsh program [3]. This is Mesh 1, with $N_E = 35,258$.

Table 3: Discretization parameters for the second MMS problem.

Parameter	Mesh 1	Mesh 2	Mesh 3
N_E	35,258	64,487	92,658
N_K	6,870	12,060	17,020
N_μ	16	16	16
N_ϕ	32	32	32

Because this is quite a tricky expression, we will be satisfied to calculate the fluence and angular distribution numerically:

$$\varphi_k^e = \frac{2\pi}{N_\phi} \sum_{i=1}^{N_\mu} \sum_{j=1}^{N_\phi} w_i \psi_{ijk}^e \tag{1.1.11}$$

$$f_i = N \frac{\pi}{2N_\phi} \sum_{e=1}^{N_E} \sum_{j=1}^{N_\phi} \sum_{k=1}^{N_K^e} \tau^e \psi_{ijk}^e \tag{1.1.12}$$

where N is a normalization constant, which is determined by quadrature of f_i/N. The source for this solution is:

$$s(\mathbf{r}, \hat{\mathbf{k}}) = \left[\Sigma_t - 2C(\mathbf{r} \cdot \hat{\mathbf{k}} - R)\right] \psi(\mathbf{r}, \hat{\mathbf{k}}) \tag{1.1.13}$$

Refer to Table 3 for discretization parameters. In Figure 4 we show the most coarse mesh in which this problem is solved. Then, refer to Figure 5 for fluences, Figure 6 for angular fluences at a select discrete ordinate, and Figure 7 for sources at the same discrete ordinate. Finally, 8 has angular distribution residuals and Table 4 has the L2-norms of the full residuals in each mesh.

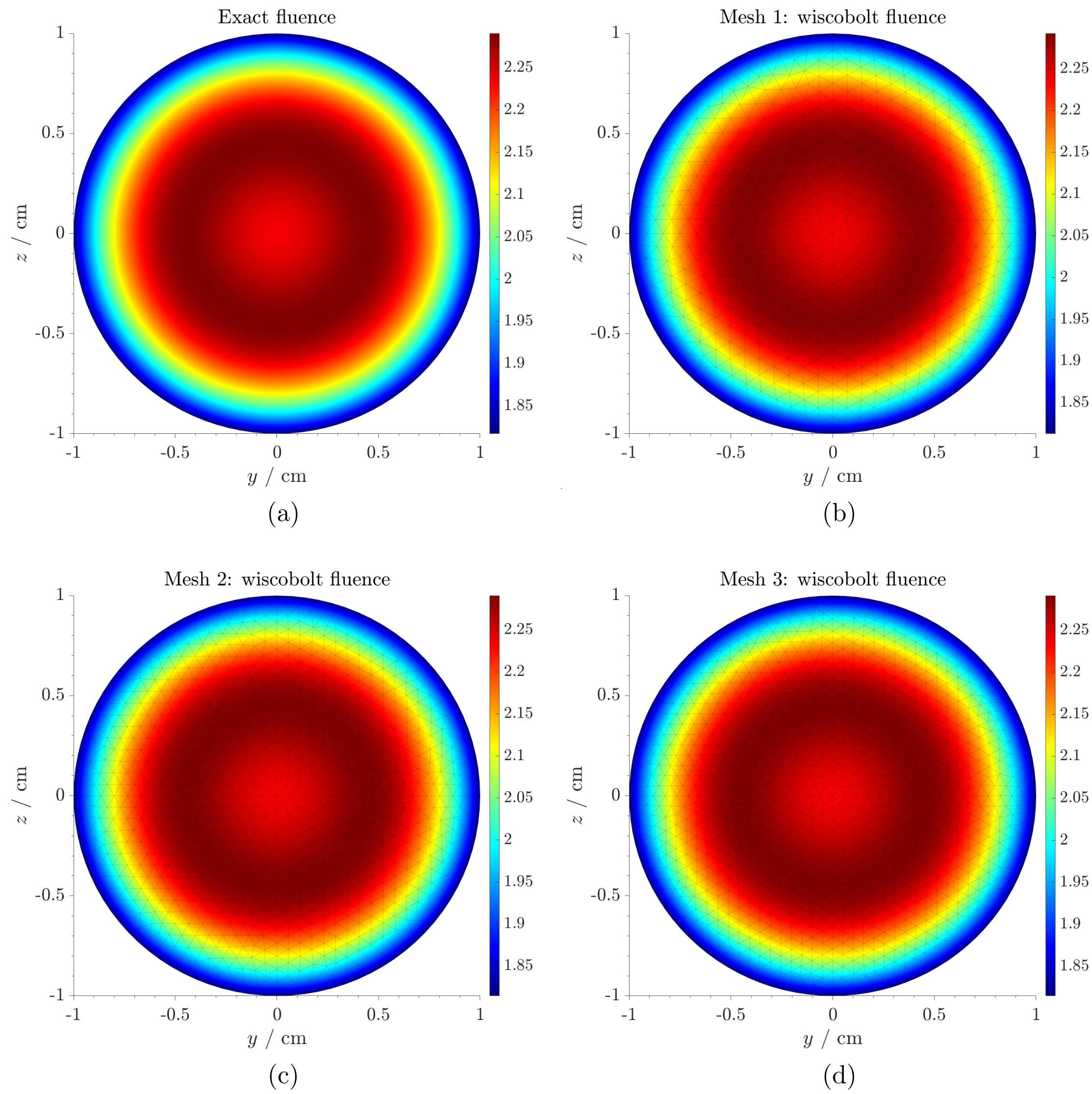

Figure 5: Figures (a)–(d) are, respectively, the exact fluence and the fluence solved by wiscobolt in meshes 1 thru 3.

Table 4: L2-norms of residuals for the second MMS problem.

	Mesh 1	Mesh 2	Mesh 3
$\lvert s - TT^{-1}s \rvert$	$5.66{\cdot}10^{-11}$	$9.30{\cdot}10^{-11}$	$1.27{\cdot}10^{-10}$

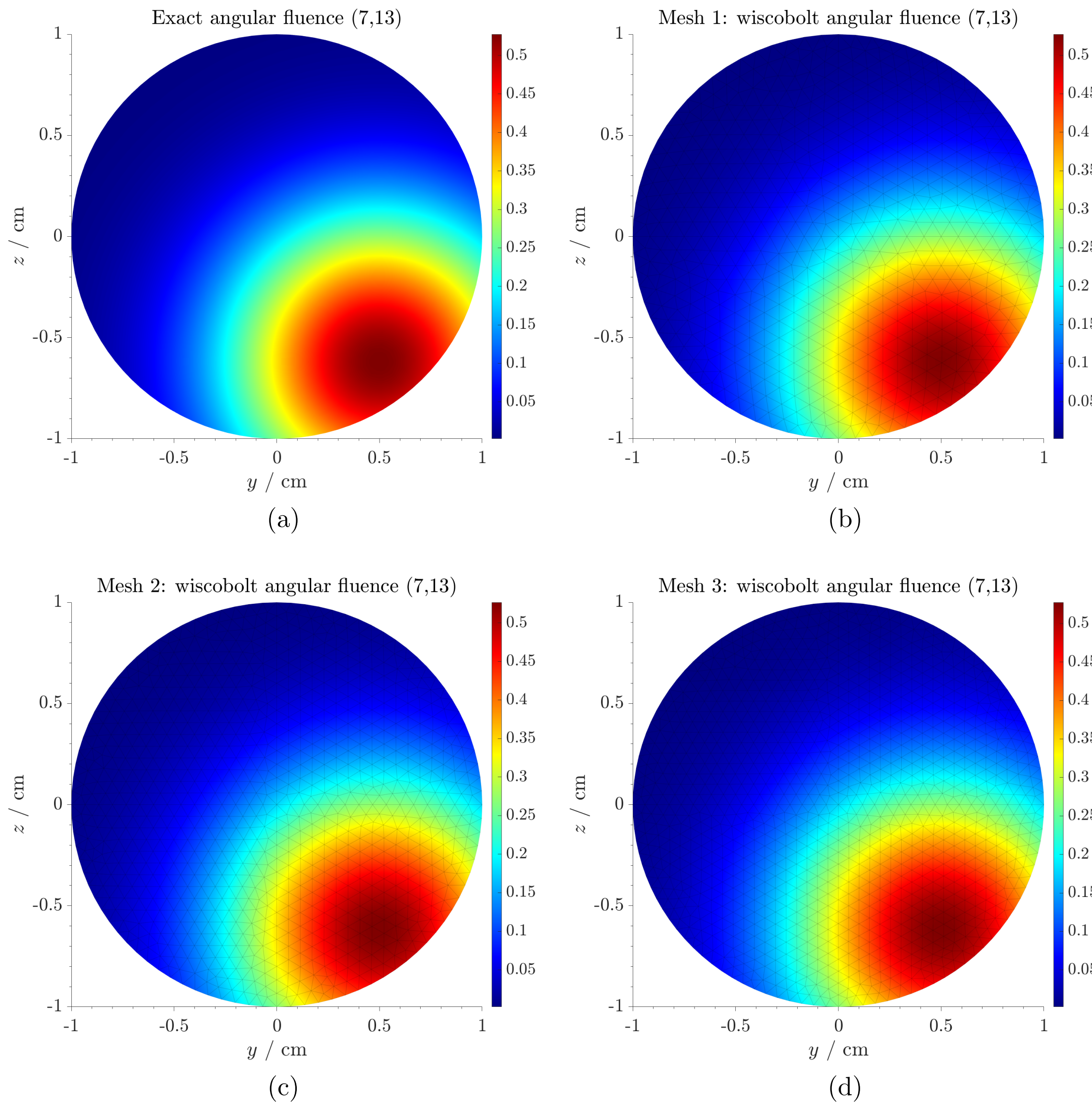

Figure 6: Figures $(a)-(d)$ are, respectively, the exact angular fluence and the angular fluence solved by wiscobolt in meshes 1 thru 3, at discrete ordinate $\hat{\mathbf{k}}_{7,13}$.

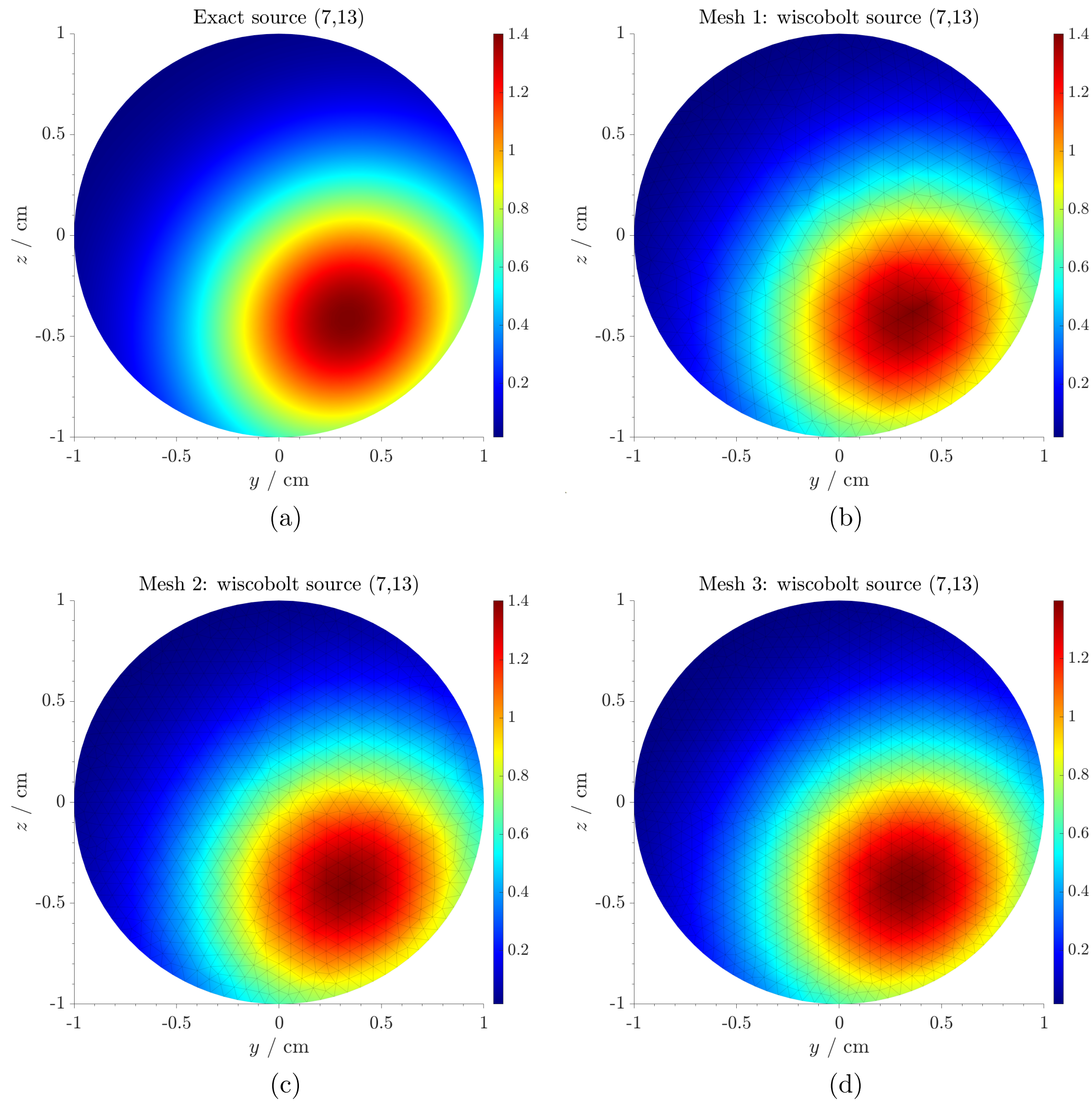

Figure 7: Figures $(a)-(d)$ are, respectively, the exact source and the source obtained by wiscobolt applying the transport operator to exact fluences in meshes 1 thru 3, at discrete ordinate $\hat{\mathbf{k}}_{7,13}$.

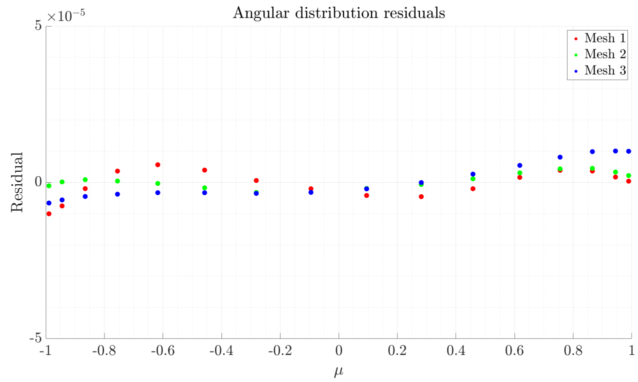

Figure 8: The residual of the angular distributions for the given meshes.

1.1.3 Test case 3 (cube, large boundary conditions)

Now, we look at a problem wherein our boundary conditions are large over all angles generally. We take:

$$\psi(\mathbf{r},\hat{\mathbf{k}}) = e^{-\cos\phi}e^{\mu}e^{-A(x-1/2)^2}e^{-A(y-1/2)^2}\left[2-\cos(\alpha z-\alpha/2)\right] \tag{1.1.14}$$

with the same values of A and α as in the first test case. The source for this problem is:

$$s(\mathbf{r},\hat{\mathbf{k}}) = \psi(\mathbf{r},\hat{\mathbf{k}}) \times \Bigg[\begin{array}{c} -A\sqrt{1-\mu^2}\cos\phi(2x-1) \\ -A\sqrt{1-\mu^2}\sin\phi(2y-1) \\ +\mu\alpha\frac{\sin(\alpha z-\alpha/2)}{2-\cos(\alpha z-\alpha/2)} \\ +\Sigma_t \end{array} \Bigg] \tag{1.1.15}$$

The angular distribution is identical to the first test problem. The fluence follows with $\cosh \to \cos$.

Refer back to Table 1 for discretization parameters. Refer to Figure 9 for solutions and Figure 10 for sources. Refer to Figure 11 for residuals of the angular distribution. Finally, refer to Table 5 for norms.

Table 5: L2-norms for the third MMS problem.

	Mesh 1	Mesh 2	Mesh 3
$\lvert s-\hat{T}\hat{T}^{-1}s\rvert$	$1.74{\cdot}10^{-10}$	$7.34{\cdot}10^{-10}$	$5.83{\cdot}10^{-9}$

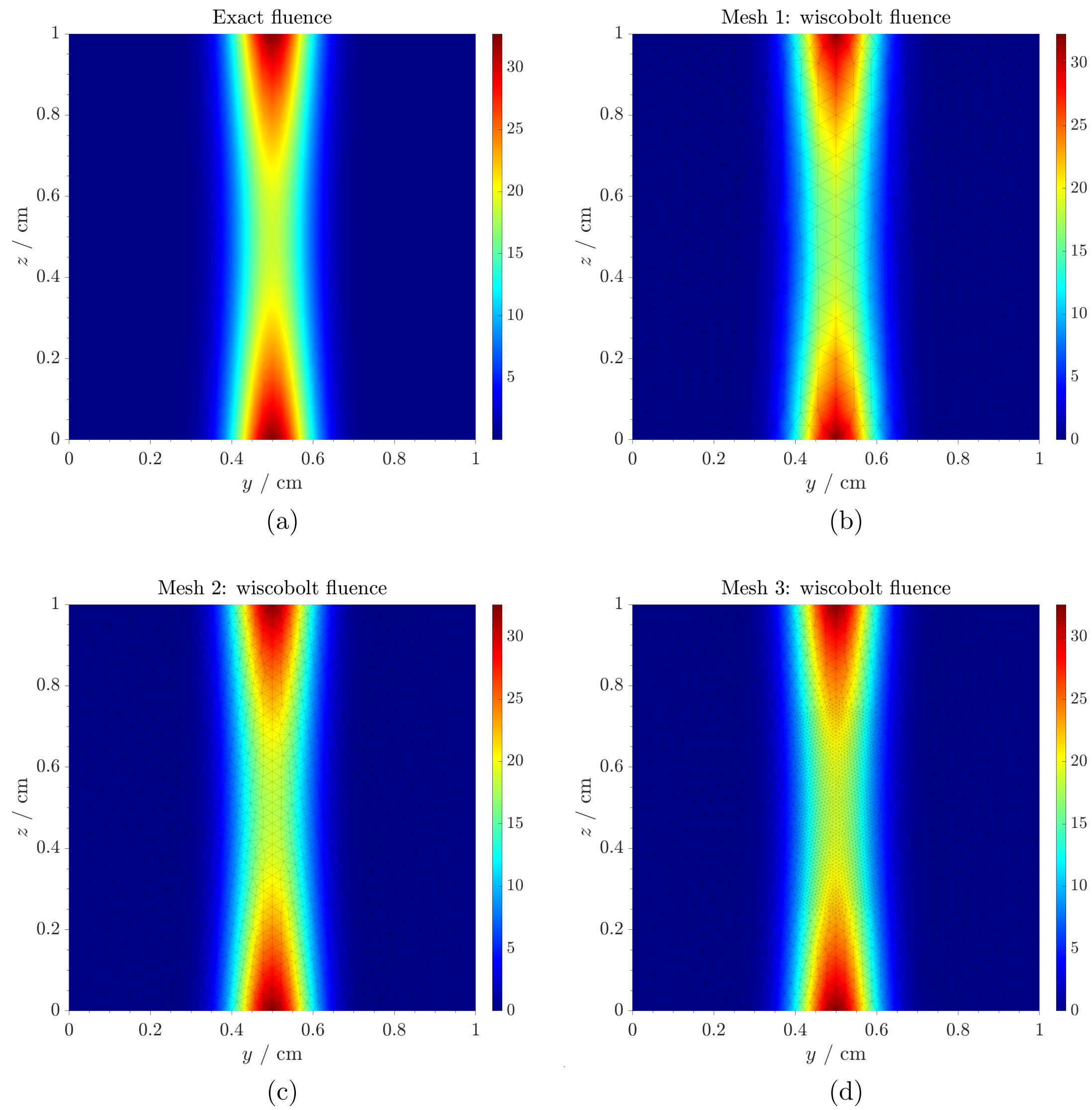

Figure 9: Figures (a)–(d) are, respectively, the exact fluence and the fluence solved by wiscobolt in meshes 1 thru 3.

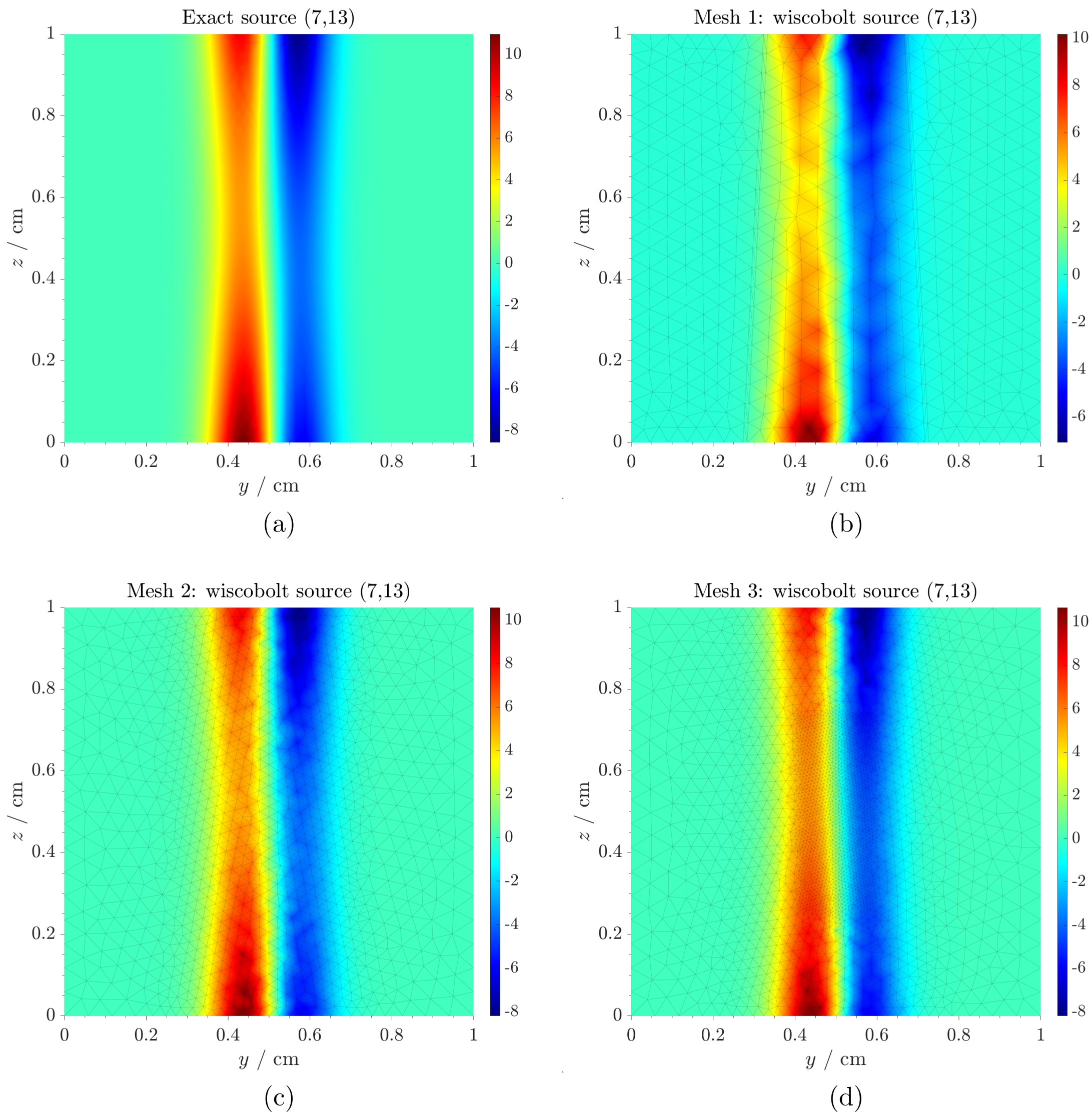

Figure 10: Figures $(a)-(d)$ are, respectively, the exact source and the source obtained by wiscobolt applying the transport operator to exact fluences in meshes 1 thru 3, at discrete ordinate $\hat{\mathbf{k}}_{7,13}$.

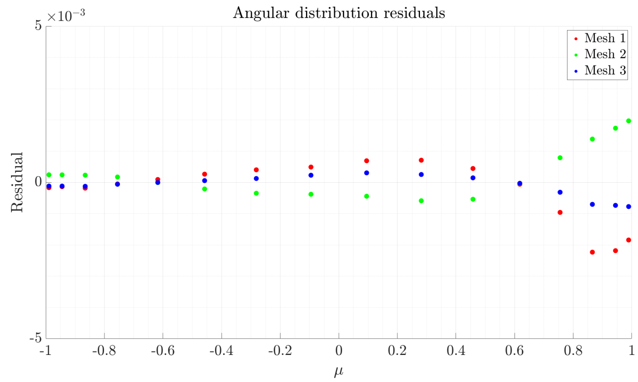

Figure 11: The residual of the angular distributions for the given meshes.

1.2 Full Boltzmann transport operator

1.2.1 Test case 1 (cube, steep gradient, vacuum boundary conditions)

The solution will be identical to the first test case of the transport operator MMS. However, for this problem, we'll have a nonzero scattering cross section:

$$\Sigma_s(\mu) = e^{\mu} \tag{1.2.1}$$

This cross section is very well represented with $L = 7$, as can be demonstrated by comparing e^x to a Taylor expansion up to x^7 over the interval $[-1, 1]$. Now, we will not analytically write $\hat{K}\psi$, instead wiscobolt will create a source term numerically:

$$s_K \equiv \sum_{\ell=0}^{L} \sum_{m=-\ell}^{\ell} \Sigma_{s,\ell} y_\ell^m(\mu, \phi) \psi_\ell^m \tag{1.2.2}$$

where ψ_ℓ^m is determined numerically via quadrature. That means we are, incorrectly, taking the 'exact' source as being determined with a truncated scattering operator and approximate angular fluence moments. However, given that the angular dependence of both ψ and Σ_s are well represented to low Legendre order, this isn't a major confounding factor to verification. Note that this problem uses vacuum boundary conditions.

We will also use the attenuation coefficient:

$$\Sigma_t = \frac{1}{c}\Sigma_{s,0} \tag{1.2.3}$$

where:

$$\Sigma_{s,0} = 2\pi(e^1 - e^{-1}) \tag{1.2.4}$$

and c is definitionally the scattering ratio $c \equiv \Sigma_{s,0}/\Sigma_t$. Effectively, when c is much less than one, there is more 'absorption' present in the problem. We'll use $c = 0.9$, so $\Sigma_t \approx 16.40$.

Table 6: L2-norms for the fourth MMS problem. Notably, they are all just below the convergence criterion of 10^{-8}, this is of course by design.

	Mesh 1	Mesh 2	Mesh 3
$\lvert s - \hat{L}\hat{L}^{-1}s \rvert$	$9.98 \cdot 10^{-9}$	$9.87 \cdot 10^{-9}$	$9.67 \cdot 10^{-9}$

Now, the non-scattering source for this problem is the same as (1.1.6):

$$s(\mathbf{r},\hat{\mathbf{k}}) - s_K(\mathbf{r},\hat{\mathbf{k}}) = \psi(\mathbf{r},\hat{\mathbf{k}}) \times \Bigg[\begin{array}{c} -A\sqrt{1-\mu^2}\cos\phi(2x-1) \\ -A\sqrt{1-\mu^2}\sin\phi(2y-1) \\ -\mu\alpha\frac{\sinh(\alpha z-\alpha/2)}{2-\cosh(\alpha z-\alpha/2)} \\ +\Sigma_t \end{array} \Bigg] \tag{1.2.5}$$

Note finally that these solutions are performed with GMRES, with a convergence criterion of 10^{-8}, but could just as easily have been performed with source iteration.

Refer back to Table 1 for discretization parameters. Refer to Figure 12 for solutions and Figure 13 for sources. Note that the discrete ordinate at which sources are evaluated is now chosen as $(i, j) = (13, 21)$, this being because the source at this ordinate shows mixing of the angular moments of the angular fluence. Refer to Figure 14 for residuals of the angular distribution. Finally, refer to Table 6 for norms.

2 Validation of physics modules (ongoing): Select results

wiscobolt includes its own modules for generating and discretizing electron and photon scattering cross sections. These cross sections will be described thoroughly in a **wiscobolt physics** document in the near future. As of now, however, according to what few head-to-head comparisons have been performed (which have thus far been confined to 1D solves in infinite slab geometry), these modules may not be capable of producing accurate energy/dose and charge deposition calculations. As of the 0.1 version, this is the primary area of focus in the development of wiscobolt, and the primary reason for which this initial release is considered a kind of alpha release. The issues, at the moment, are apparently a slight overestimation of energy/dose and charge deposition in homogeneous media, as well as underestimation downstream of material inhomogeneities, and significant differences in deposition across different methods (i.e., different forms of the RCSDA operator, MGXS vs. FEXS). It is for this reason that the user has the option to input their own physics cross sections, as described in **wiscobolt implementation**.

We will show nonetheless what wiscobolt's physics modules are currently able to produce with MGXS energy discretization. In general, however, it is planned that every validation study eventually performed will reach agreement with Monte Carlo calculations.

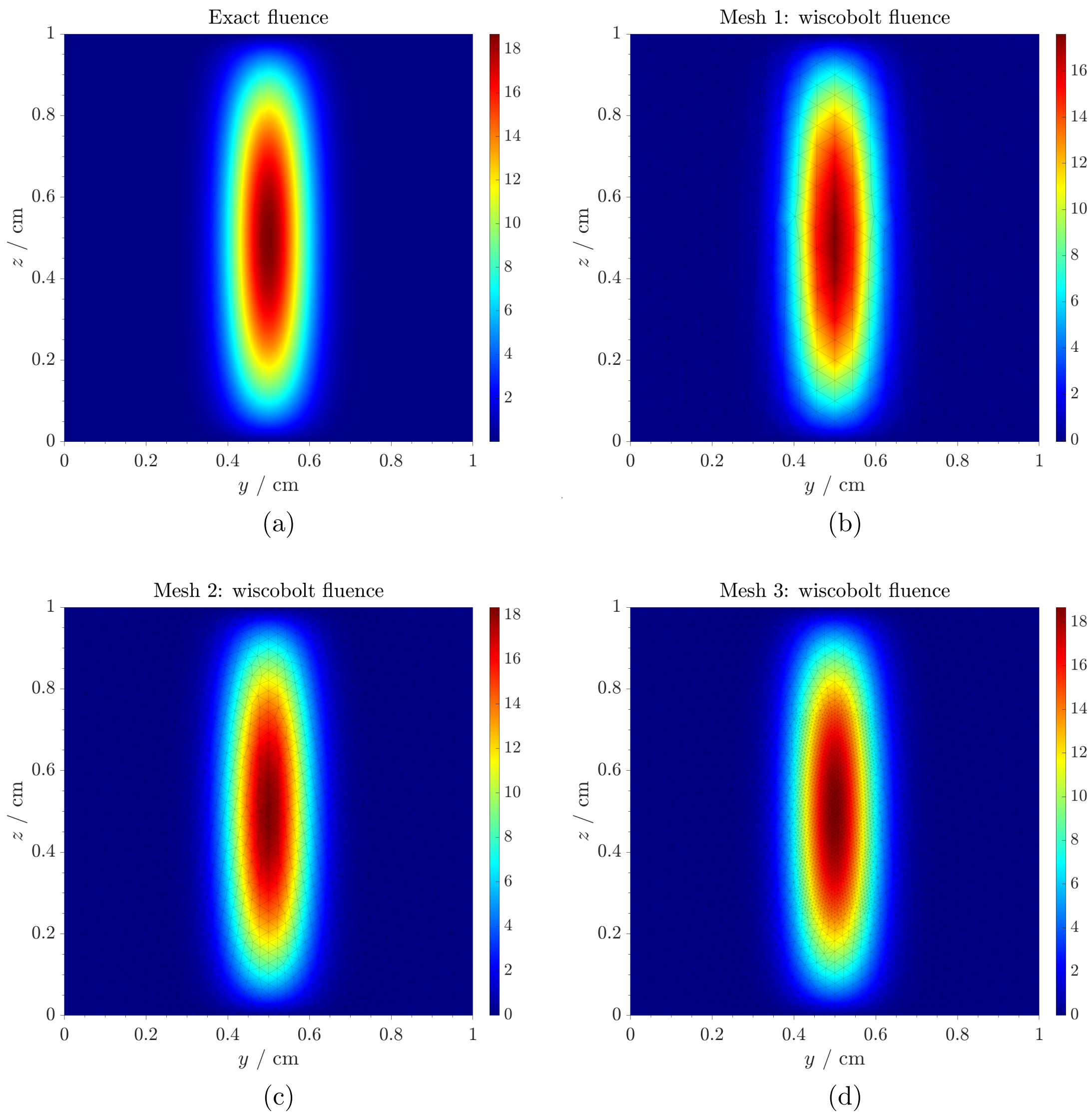

Figure 12: Figures (a)–(d) are, respectively, the exact fluence and the fluence solved by wiscobolt in meshes 1 thru 3.

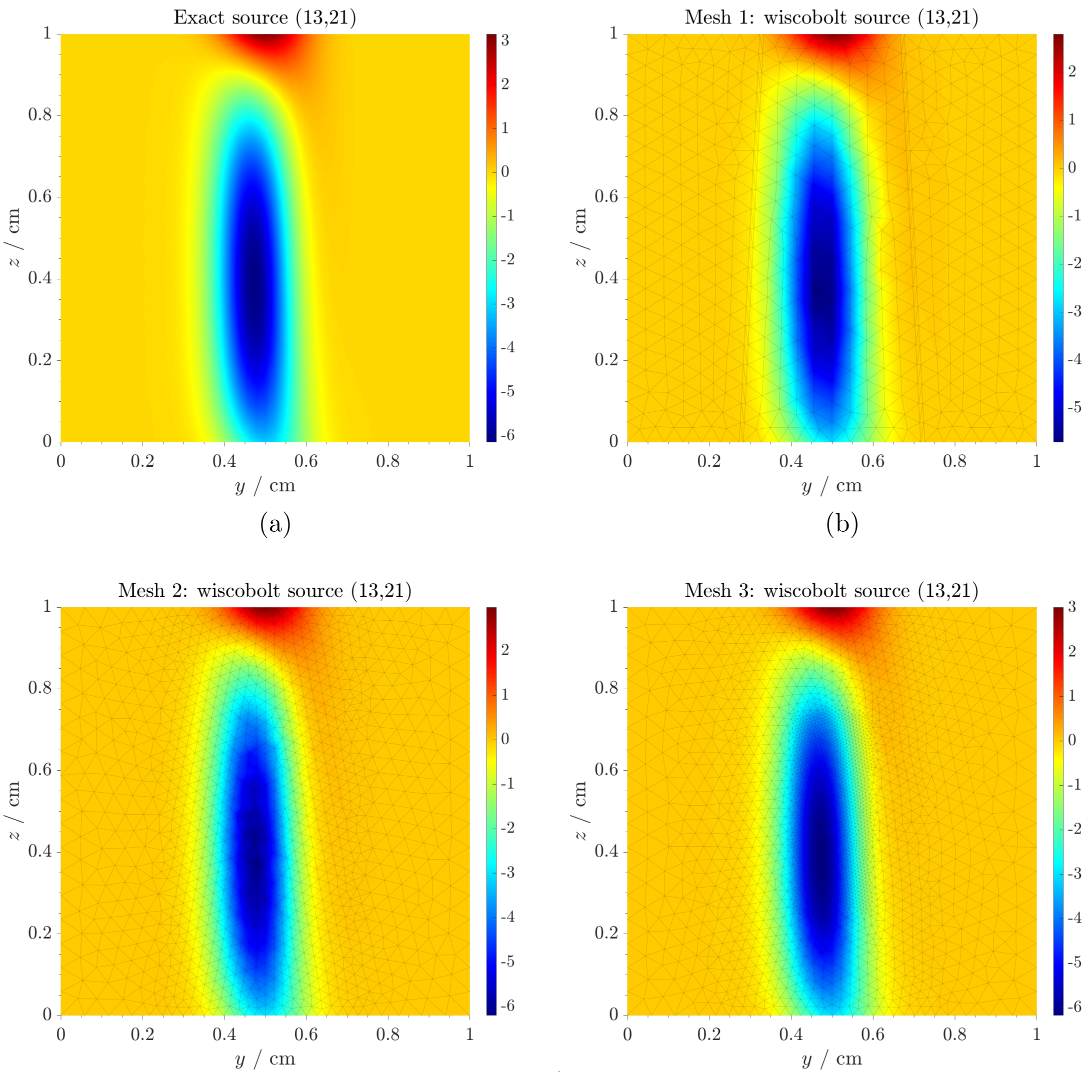

(a) (b) (c) (d)

Figure 13: Figures $(a){-}(d)$ are, respectively, the exact source and the source obtained by wiscobolt applying the transport operator to exact fluences in meshes 1 thru 3, at discrete ordinate $\hat{\mathbf{k}}_{13,21}$.

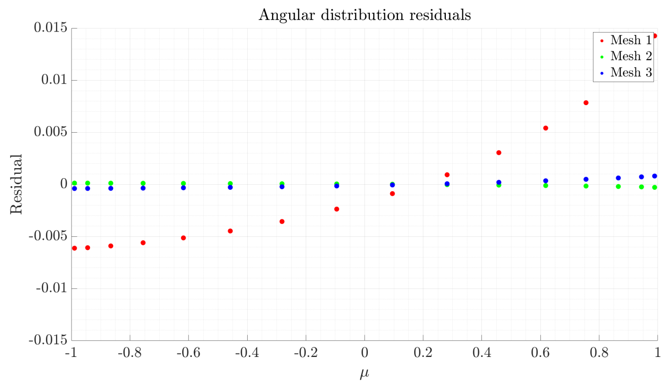

Figure 14: The residual of the angular distributions for the given meshes.

Note that the electron solutions about to be shown were created using MGXS energy discretization, Möller scattering, the first-order RCSDA differencing, and elastic scattering cross sections generated by the ELSEPA program [4]. Additionally, photon solutions have also been created using MGXS, however, agreement between MGXS and FEXS discretization methods for photons has been achieved by wiscobolt.

2.1 Open 1 MeV electron beam on Aluminum

This problem consists of monoenergetic, 1 MeV electrons incident normally on an aluminum slab of thickness 0.2 cm and a width of only 1 cm. This geometry is depicted in **Figure 16**.

The definition of a 'monoenergetic' beam in MGXS is taken as follows: with G energy groups, with E_{min} cutoff energy, a monoenergetic beam of energy E_0 is created by using linearly spaced groups with minimum energy E_{min}, and a maximum energy such that the midpoint energy of the first energy group is E_0, then populating only energy group 1. For example, with $G = 25$, $E_{\text{min}} = 1$ keV, and $E_0 = 1$ MeV, one finds the energy spectrum in **Figure 15**.

We use $N_E = 220,885$. However, this may be a bit too coarse to accurately treat the variation of the solution in the axial dimension. Now, as we are using the FCS with beam quadrature (which is described in the main **wiscobolt** document), this is not concerning for the magnitude of the solution, but rather its refinement around mesh elements in regions with a steep gradient.

Nevertheless, the dose deposition in a mesh slice is shown in **Figure 17** with the mesh slice overlain.

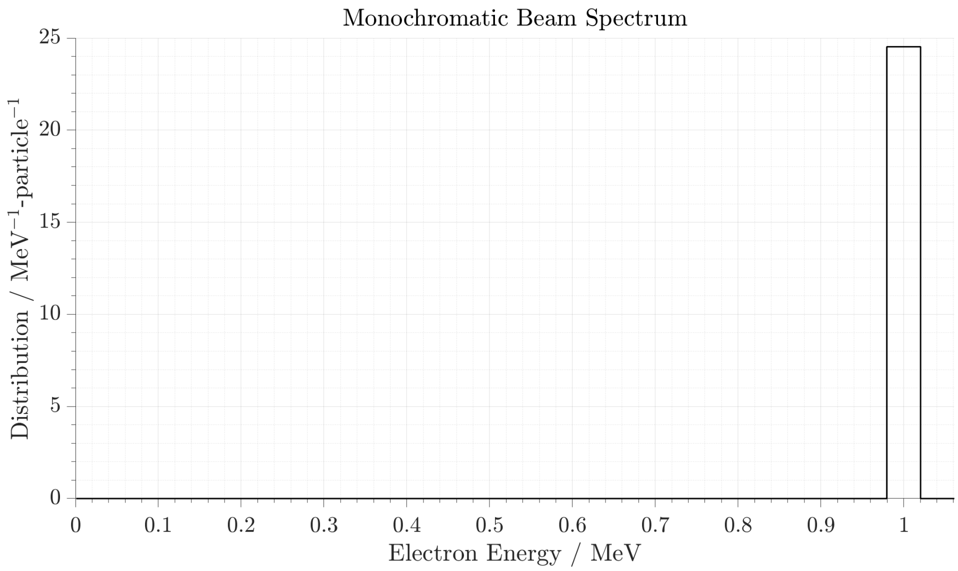

Figure 15: Energy distribution of incident electrons.

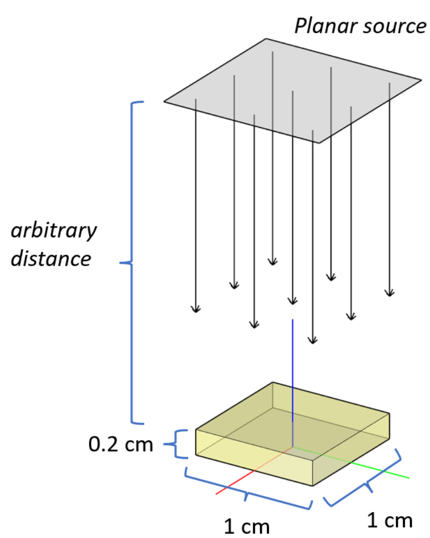

Figure 16: Geometry of this problem. Red/green/blue axes are the $x-$, $y-$, and $z-$axes respectively. Direction of incidence is indicated by arrows. Beam-covered volume is colored yellow.

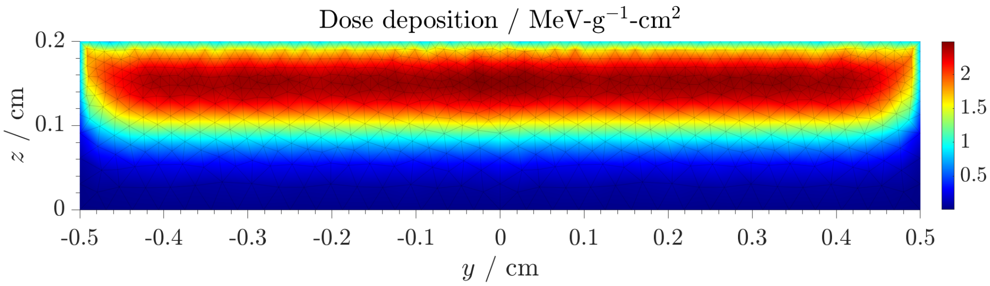

Figure 17: Dose deposition in a mesh slice due to the previously described beam and geometry. The mesh slice is overlain to demonstrate that, when such a thin mesh is used, axial resolution is not as finely tuned, even with ∼220,000 elements. Ideally, the mesh size closer to the surface would be substantially more dense.

2.2 Narrow 1 MeV electron beam on Aluminum

This problem consists of 1 MeV electrons incident normally on an aluminum slab of thickness 0.2 cm and a width of only 0.5 cm. This geometry is depicted in **Figure 18**. The mesh is depicted in **Figure 19** The energy distribution is the same as **Figure 15**. In this case, we are going to use a narrow planar beam, specifically one that is 0.05×0.05 cm^2. wiscobolt can generate the mesh-slice dose deposition in **Figure 20**.

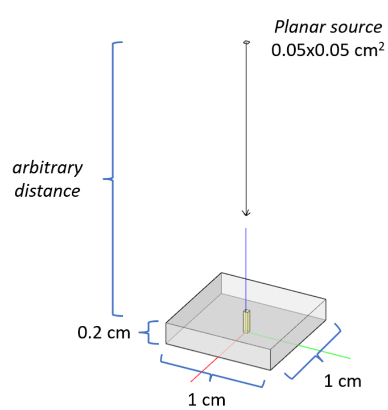

Figure 18: Geometry of this problem.

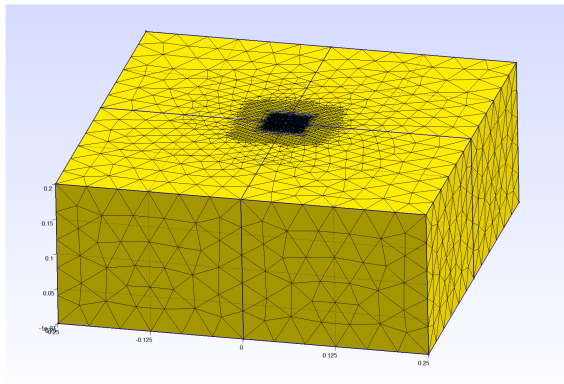

Figure 19: Mesh of a $0.5 \times 0.5 \times 0.2$ slab with a planar beam of 0.05×0.05. Mesh is refined in a rectangular prismatic region about the beam, and particularly refined in at more shallow depths. Units assigned by wiscobolt as cm. Mesh created by Gmsh program.

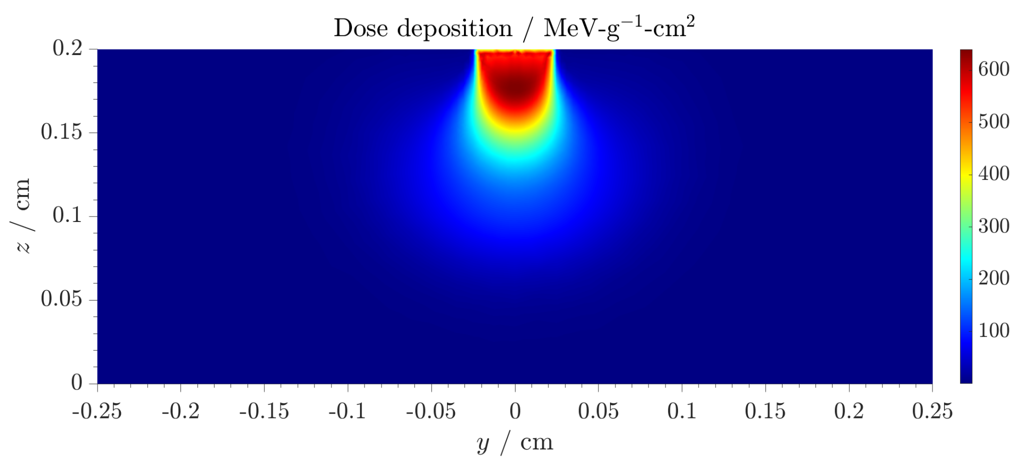

Figure 20: Dose deposition in a mesh slice due to the previously described beam and geometry.

2.3 6MV therapeutic electron beam on water slab

The spectrum used for this problem is a 6MV therapeutic electron beam, shown in **Figure 21** in its interpolated and energy-grouped form. The geometry, depicted in **Figure 22**, is a spherical beam at a distance of 100 cm from the surface of a 30 × 30 × 5 cm^3 water tank, which is collimated to 10×10 cm^2 at the surface. wiscobolt can generate the mesh-slice dose deposition in water that is shown in **Figure 23**.

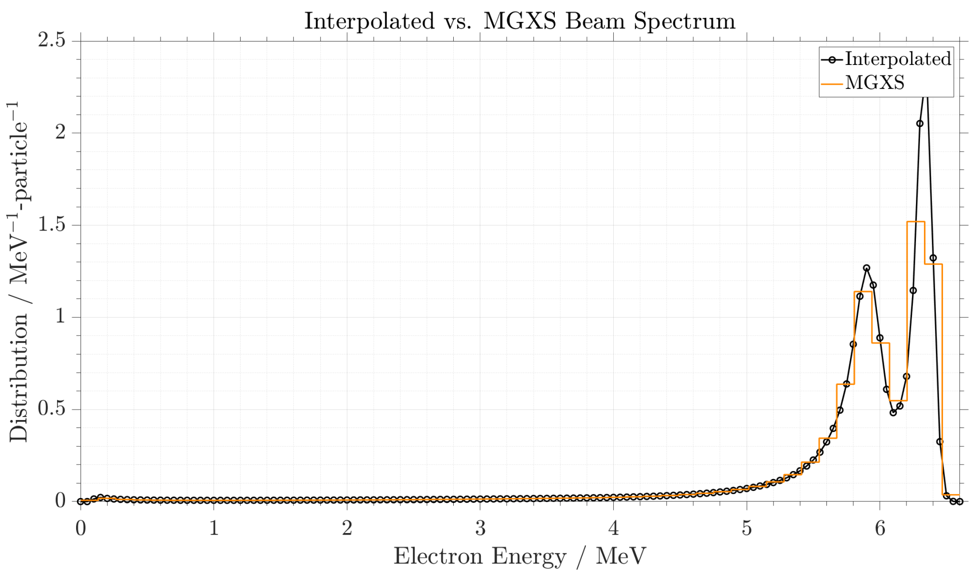

Figure 21: Energy distribution of incident electrons in its linearly interpolated form, and in its MGXS-discretized form with 50 electron energy groups.

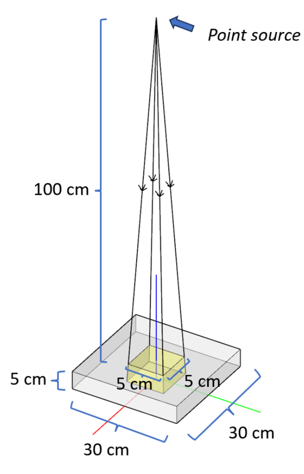

Figure 22: Geometry of this problem.

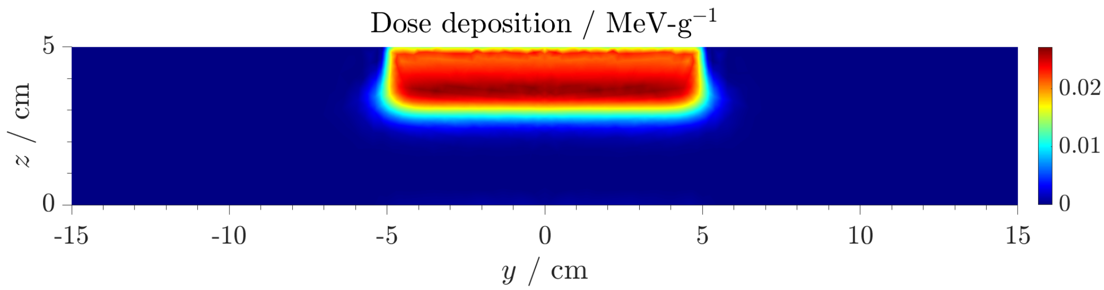

Figure 23: Dose deposition in a mesh slice due to the previously described beam and geometry.

2.4 6MV therapeutic photon beam on water cube

The spectrum used for this problem is a 6MV therapeutic photon beam, shown in **Figure 24** in its interpolated and energy-grouped form. The geometry, depicted in **Figure 25**, is a spherical beam at a distance of 100 cm from the surface of a $30 \times 30 \times 30$ cm^3 water tank, which is collimated to 10×10 cm^2 at the surface. The mesh, up to a scale factor of 30 in each dimension, is shown in **Figure 26** Now, the depth-dose deposition curves that wiscobolt generates are having trouble in that dose deposition is just far too shallow. The cause of this problem is likely due to the discretization of photon-electron cross sections. Instead of performing an electron calculation and showing the dose, we will demonstrate what wiscobolt can produce as far as fluence maps, and show that wiscobolt can accurately describe the tendency for low energy X-rays to undergo large-angle scattering.

Collided fluences for certain energy groups in a mesh-slice are shown in **Figure 27**.

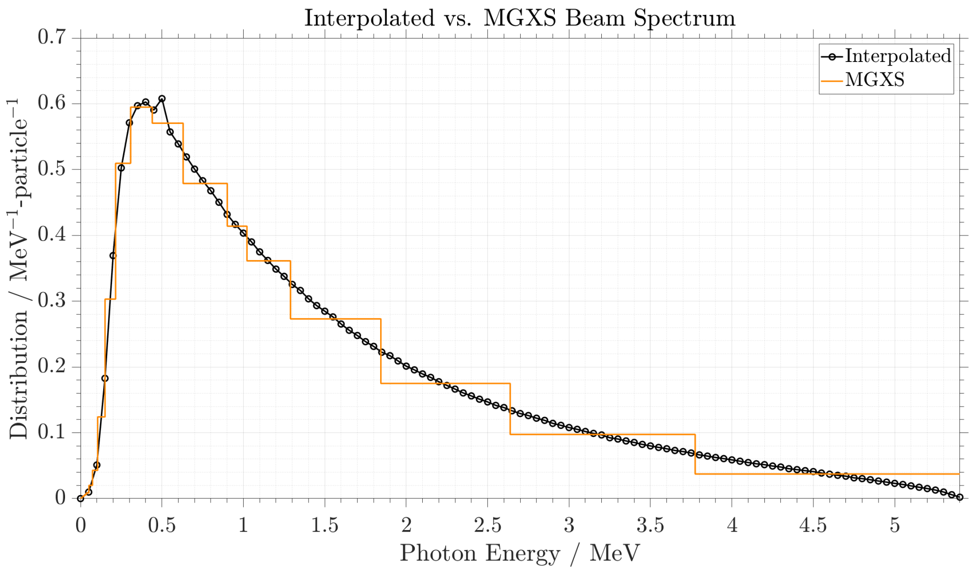

Figure 24: Energy distribution in its interpolated and energy-grouped form. We use 25 energy groups with logarithmic spacing, the only exception being that we force an energy node to exist at 1.022 MeV, which is done to accommodate pair-production in this problem.

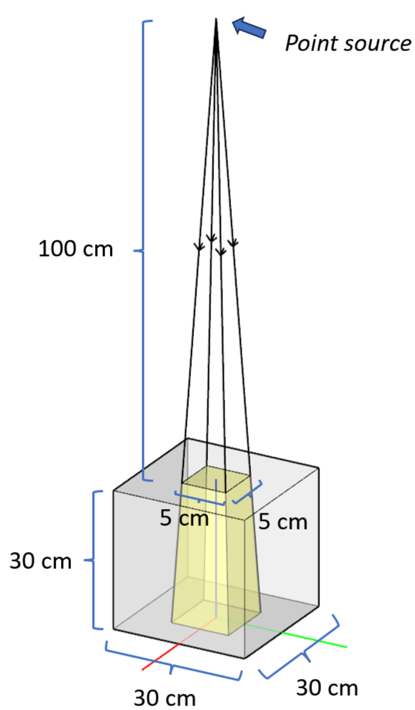

Figure 25: Geometry of this problem.

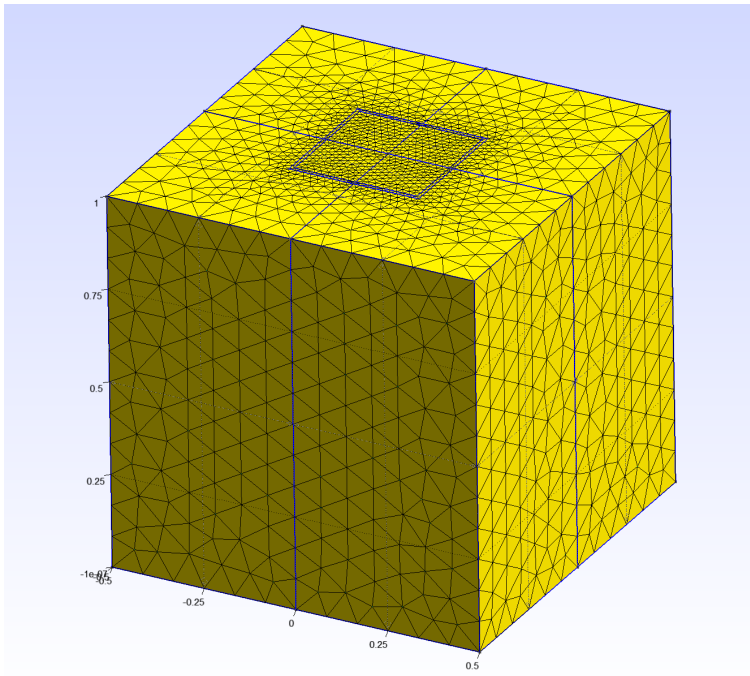

Figure 26: Mesh of a $1 \times 1 \times 1$ cube. Includes a spherical beam, a distance of $10/3$ away from the surface of the cube, with $1/3 \times 1/3$ field size at the surface. Units are assigned by wiscobolt as 30 cm using the "scale mesh" option in the input file and providing a scale vector $[30, 30, 30]$. Mesh created by Gmsh program.

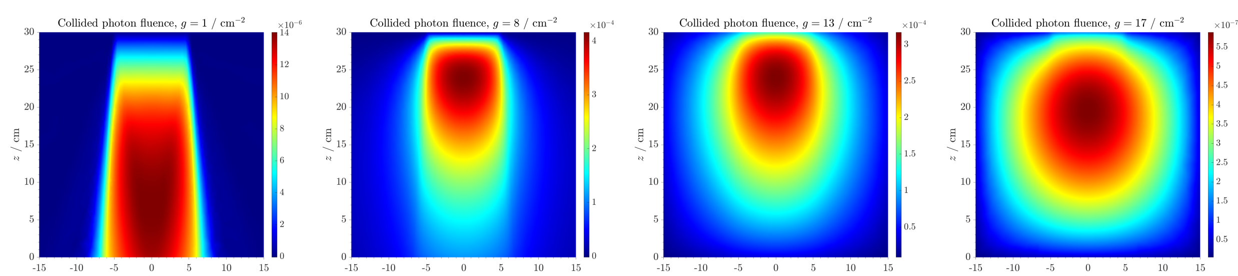

Figure 27: Collided photon fluence in a mesh slice for various energy groups. Note that the gth fluence represents the total fluence in that group, i.e., the typical fluence integrated over energy. The chosen groups, and their respective energy ranges in MeV, are $g = 1$ $(3.77 - 5.40), 8$ $(0.440 - 0.630), 13$ $(0.073 - 0.105), 17$ $(0.018 - 0.025)$.

2.5 6MV therapeutic photon beam on water slab

This problem is going to be identical to the previous one, only now the geometry is a $30 \times 30 \times 15$ cm^3 slab. The mesh is shown in **Figure 28**.

Collided fluences for certain energy groups in a mesh-slice are shown in **Figure 29**.

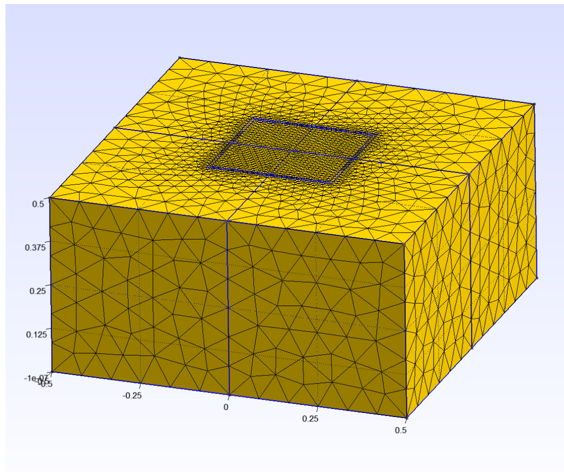

Figure 28: Mesh of a $1 \times 1 \times 0.5$ slab. Includes a spherical beam, a distance of 10/3 away from the surface of the cube, with $1/3 \times 1/3$ field size at the surface. Units are assigned by wiscobolt as 30 cm using the "scale mesh" option in the input file and providing a scale vector $[30, 30, 30]$. Mesh created by Gmsh program.

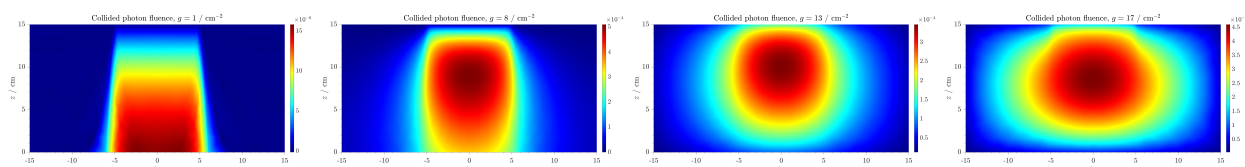

Figure 29: Collided photon fluence in a mesh slice for various energy groups. The chosen groups, and their respective energy ranges in MeV, are $g = 1$ $(3.77 - 5.40), 8$ $(0.440 - 0.630), 13$ $(0.073 - 0.105), 17$ $(0.018 - 0.025)$. In comparison to **Figure 27**, this is an interesting demonstration of the tendency of lower energy photons to backscatter. When the medium is made smaller in the longitudinal dimension, fluence of high energy photons downstream of the beam is similar to what it originally had been. Conversely, for low energy photons, the fluence still drops to near-zero downstream of the beam.

References

[1] P. J. Roache, "Code verification by the method of manufactured solutions", Journal of Fluids Engineering **124**, 4 (2002).

[2] J. Wang, W. Martin, and B. Collins, "The application of method of manufactured solutions to method of characteristics in planar geometry", Annals of Nuclear Energy **121**, 295 (2018).

[3] C. Geuzaine and J. Remacle, "Gmsh: a three-dimensional finite element mesh generator with built-in pre- and post-processing facilities.", International Journal for Numerical Methods in Engineering **79**, 1309 (2009).

[4] F. Salvat, A. Jablonski, and C. J. Powell, "ELSEPA - dirac partial-wave calculation of elastic scattering of electrons and positrons by atoms, positive ions, and molecules", Computer Physics Communications **261**, 107704 (2005).